Cx43-mediated sorting of miRNAs into extracellular vesicles

Tania Martins-Marques[1,2,3] (iD), Marina C Costa[4], Steve Catarino[1,2,3] (iD), Isaura Simoes[2,5,6], Trond Aasen[7,8], Francisco J Enguita[4] (iD) & Henrique Girao[1,2,3,*] (iD)

Abstract

Through the exchange of lipids, proteins, and nucleic acids, extracellular vesicles (EV) allow for cell–cell communication across distant cells and tissues to regulate a wide range of physiological and pathological processes. Although some molecular mediators have been discovered, the mechanisms underlying the selective sorting of miRNAs into EV remain elusive. Previous studies demonstrated that connexin43 (Cx43) forms functional channels at the EV surface, mediating the communication with recipient cells. Here, we show that Cx43 participates in the selective sorting of miRNAs into EV through a process that can also involve RNA-binding proteins. We provide evidence that Cx43 can directly bind to specific miRNAs, namely those containing stable secondary structure elements, including miR-133b. Furthermore, Cx43 facilitates the delivery of EV-miRNAs into recipient cells. Phenotypically, we show that Cx43-mediated EV-miRNAs sorting modulates autophagy. Overall, our study ascribes another biological role to Cx43, that is, the selective incorporation of miRNAs into EV, which potentially modulates multiple biological processes in target cells and may have implications for human health and disease.

Introduction

Extracellular vesicles (EV) are nanosized particles that act as major vehicles for exchange of information across distant cells and tissues, without requiring cell-to-cell contact (Wolf, 1967; Ribeiro-Rodrigues *et al*, 2017b). EV can carry a wide variety of macromolecules, including lipids, proteins, mRNA, and microRNAs (miRNAs). An increasing attention has been given to EV-enclosed miRNAs, because of their role in modulating multiple biological processes in target cells, including cell senescence, angiogenesis, and autophagy, involved in diverse human diseases (Balkom *et al*, 2013; Ribeiro-Rodrigues *et al*, 2017a; Zhou *et al*, 2019).

Although initially considered as a rather random process, ample evidence now indicates that the EV-mediated flow of information is highly specific and regulated, with the sorting of signaling molecules, namely miRNAs, being thoroughly scrutinized during EV biogenesis. The first protein to be implicated in miRNAs delivery to EV was heterogeneous nuclear ribonucleoprotein (hnRNP)-A2B1, whose sumoylation regulated selective recognition and incorporation of miRNAs into EV (Villarroya-Beltri *et al*, 2013). Later, synaptotagmin binding cytoplasmic RNA interacting protein (SYNCRIP; also known as hnRNPQ), Y-box protein (YBX)-1, major vault protein (MVP), human antigen R (HuR), Mex-3 RNA binding family member C (MEX3C), Lupus La protein, Alyref, and Fus were also demonstrated to select miRNAs to be delivered into EV (Mukherjee *et al*, 2016; Santangelo *et al*, 2016; Shurtleff *et al*, 2016; Teng *et al*, 2017; Hobor *et al*, 2018; Temoche-Diaz *et al*, 2019; Garcia-Martin *et al*, 2022). For hnRNPA2B1, hnRNPQ and La protein, primary sequences for miRNAs recognition were identified (GGAG, GGCU and UUU, respectively), all of them being preferentially localized in the 3′-end of miRNAs (Villarroya-Beltri *et al*, 2013; Santangelo *et al*, 2016; Temoche-Diaz *et al*, 2019). These findings suggest that different RNA-binding proteins display sequence-specific EV sorting capacities, which may underlie cell type- or stimulus-specific mechanisms (Garcia-Martin *et al*, 2022). On the other hand, Koppers-Lalic *et al* (2014) demonstrated that post-transcriptional modifications on miRNAs, namely 3′-end uridylation, modulate their selective incorporation into EV.

Several studies have further demonstrated that miRNAs sorting is highly determined by the cellular physiological state. For

example, cell activation-induced changes in the levels of miRNAs target levels in EV-producing cells were shown to modulate the enrichment of miRNAs in secreted EV (Baer *et al*, 2014). Moreover, aberrant KRAS signaling was described to induce phosphorylation of protein argonaute 2 (Ago2), with a consequent increased secretion of specific Ago2-miRNAs complexes into EV (McKenzie *et al*, 2016). More recently, the membrane protein caveolin-1 was shown to control the traffic of hnRNPA2B1-miRNAs complexes towards EV under oxidative stress, while the autophagy protein LC3 was involved in loading diverse RNA-binding proteins into vesicles, thereby modulating their RNA landscape (Lee *et al*, 2019; Leidal *et al*, 2020). Despite inaugural studies have shed some light on the molecular mechanisms and signaling pathways involved in the selective package of miRNA, this is a topic that is now in its infancy with many unexplored aspects demanding further elucidation. Given the complexity and selectivity of the process, it is likely that other proteins, namely membrane proteins, contribute to miRNAs sorting into EV.

Seminal studies from our group have demonstrated that the gap junction (GJ) protein connexin43 (Cx43) forms functional hexameric structures at the EV surface, which facilitates the rapid release of vesicle content into recipient cells, thus constituting an alternative mechanism of information flow between EV and target cells (Soares *et al*, 2015). Furthermore, ubiquitination, previously shown by our laboratory to target gap junctions for autophagy degradation, also signals the sorting of Cx43 into EV, suggesting an orchestrated crosstalk between autophagy and EV sorting as part of a protein quality control strategy (Martins-Marques *et al*, 2015b, 2020b). Strikingly, we unveiled that the levels of Cx43 were decreased both in EV secreted by cardiomyocytes subjected to ischemia and in circulating EV after myocardial infarction, posing as a potential disease biomarker (Martins-Marques *et al*, 2020b).

Our previous proteomic studies revealed that the Cx43 interactome includes various RNA-binding proteins with a critical role in the selective sorting of EV-miRNAs, including hnRNPA2B1 and hnRNPQ (Martins-Marques *et al*, 2015a). Moreover, several RNA-binding motifs were predicted in the Cx43 sequence, ascribing novel and unanticipated functions to this protein (Varela-Eirin *et al*, 2017). Hence, in the present work, we hypothesize that, besides its role in cell–cell communication and EV-cell interaction, Cx43 plays unconventional biological functions upon the selection of specific miRNAs for secretion.

Results

Cx43 modulates the selective sorting of miRNAs into EV

Previous studies from our lab have elucidated the mechanisms whereby Cx43 is sorted into EV, as well as the role of Cx43-containing vesicles as therapeutic vehicles (Martins-Marques *et al*, 2016, 2020b). In the present study, we hypothesized that Cx43 modulates the selective sorting of cargo into EV, namely in terms of miRNAs. To address that, we profiled the expression levels of 752 miRNAs in EV isolated from HEK293 cells expressing or not Cx43—EV^{Cx43+} or EV^{Cx43-}. Results depicted on Fig 1A show that 11 miRNAs were differentially represented in EV^{Cx43+} and EV^{Cx43-} ($P < 0.1$). Of these, 7 miRNAs were selectively enriched in EV^{Cx43+}—miR-410, miR-199a-3p, let-7d-3p, miR-133b, miR-744-3p, miR-335-3p, let-7g-5p, whereas 4 miRNAs were downregulated in EV^{Cx43+}—miR-300, miR-24-3p, miR-454-3p, miR-509-3p. In contrast, the changes in miRNAs levels between cells expressing or not Cx43 were less pronounced than in EV (Fig EV1A), suggesting that Cx43 participates in the selective sorting of EV-enclosed miRNAs. The total protein content, RNA levels, concentration or vesicle size did not present significant differences (Fig EV1B–F).

Pathway enrichment analysis associate miRNAs enriched in Cx43-containing EV with circadian rhythm, focal adhesion, autophagy, and multiple signaling pathways, including mitogen-activated protein kinase (MAPK) and Forkhead box O (FoxO) (Fig 1B). Gene ontology (GO)-term enrichment analysis links overrepresented miRNAs in EV^{Cx43+} to vascular wound healing and phosphatase activity (Fig EV2A–C). To validate our enrichment analysis *in vitro*, we proceed to assess the biological impact of EV-enclosed miRNAs, following incubation of HEK293 cells with either EV^{Cx43+} or EV^{Cx43-}, upon autophagy activation. Our results show that in cells stimulated with EV^{Cx43+}, treatment with the lysosomal inhibitor Bafilomycin A1 resulted in an increased accumulation of LC3-II, when comparing with EV^{Cx43-}, suggesting that the miRNAs repertoire of EV^{Cx43+} enhances autophagy flux (Fig 1C). In parallel, the number of GFP-LC3 puncta in serum-starved cells following incubation with EV^{Cx43+} was decreased (Fig EV3A), likely reflecting an increased lysosomal degradation of autophagic structures in recipient cells. To discard a cell-specific effect, these data were validated using EV obtained from a different cell line, C33a. Since C33a cells endogenously express Cx43, we knocked-out (KO) Cx43 using CRISPR/Cas9, after which EV were isolated from either the parental ($EV^{Cx43-WT}$) or the KO cells ($EV^{Cx43-KO}$). Results on Fig EV3B show that C33a-derived $EV^{Cx43-WT}$

Figure 1. Cx43 modulates the selective sorting of miRNAs into extracellular vesicles.

A EV produced by HEK293 cells expressing or not Cx43 (EV^{Cx43+} or EV^{Cx43-}) were purified by differential ultracentrifugation. miRNAs expression profile analysis in EV^{Cx43+} (represented as fold increase over EV^{Cx43-}).
B Pathway enrichment analysis for the predicted targets of the over-represented miRNAs in Cx43-containing EV.
C HEK293 cells were incubated with 5 μg of purified EV^{Cx43-} or EV^{Cx43+} for 24 h, in the presence or absence of Bafilomycin A1 (Baf) in the last 6 h. The levels of LC3 were analyzed by WB and are depicted on graph (LC3-II; $n = 4$ biological replicates).
D miRNA-centered regulatory network established by the miRNAs enriched in Cx43-containing EV. The figure represents predicted targets that are simultaneously regulated by 3 or more of the selected miRNAs. The size of the symbols is proportional to the number of established functional connections. miRNA-regulatory are represented by grey edges. Protein–protein interactions obtained from STRING database are depicted in black lines.
E HEK293 cells were incubated with EV^{Cx43-} or EV^{Cx43+} for 24 h before WB analysis of ATP2A2/SERCA2, a predicted target of miRNAs enriched in Cx43-containing EV. Graph depicts quantification of ATP2A2/SERCA2 levels ($n = 4$ biological replicates).

Data information: *P*-values were derived by Mann–Whitney test. Bars and error bars indicate mean ± SD in all graphs.
Source data are available online for this figure.

A

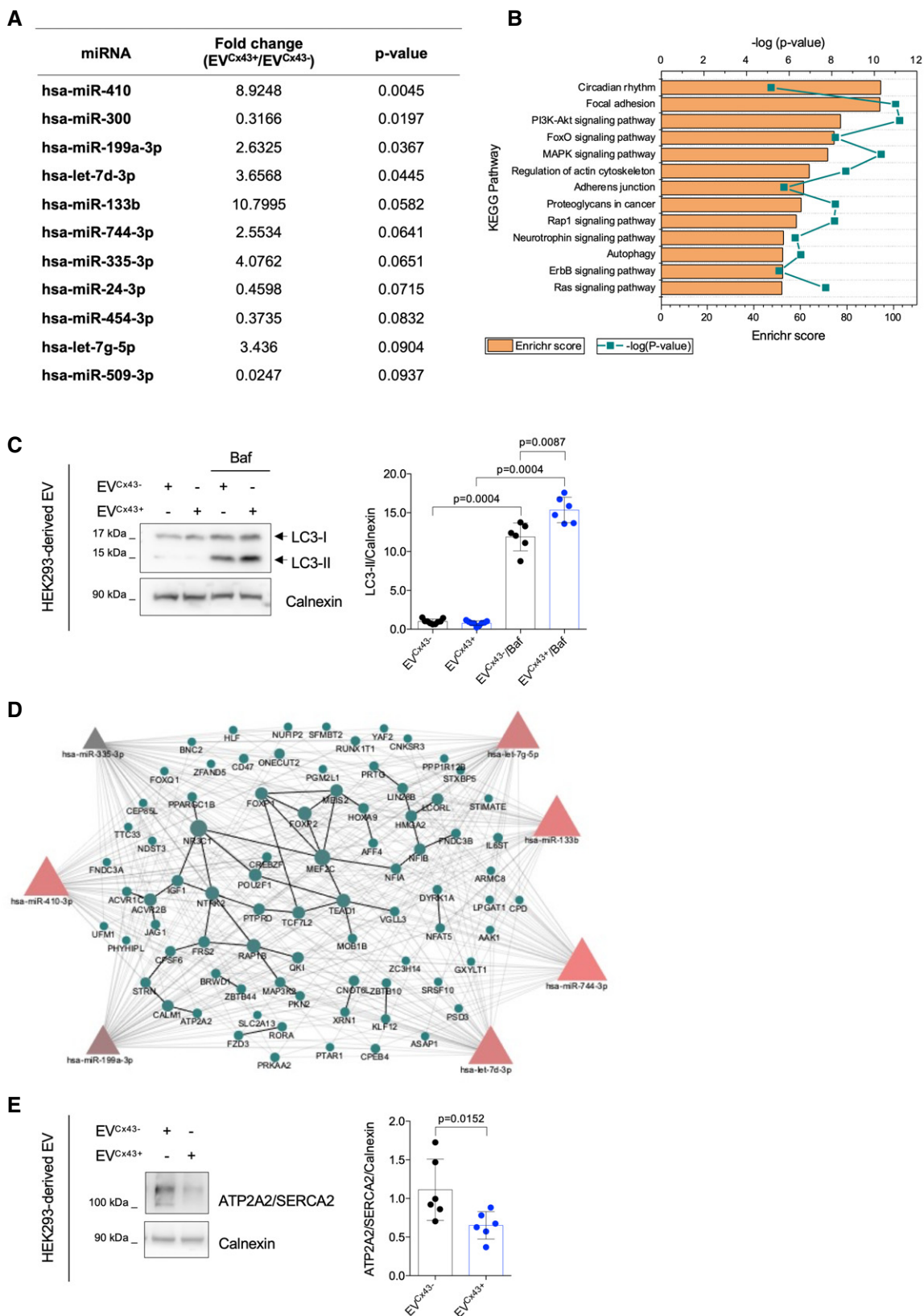| miRNA	Fold change (EV^{Cx43+}/EV^{Cx43-})	p-value
hsa-miR-410	8.9248	0.0045
hsa-miR-300	0.3166	0.0197
hsa-miR-199a-3p	2.6325	0.0367
hsa-let-7d-3p	3.6568	0.0445
hsa-miR-133b	10.7995	0.0582
hsa-miR-744-3p	2.5534	0.0641
hsa-miR-335-3p	4.0762	0.0651
hsa-miR-24-3p	0.4598	0.0715
hsa-miR-454-3p	0.3735	0.0832
hsa-let-7g-5p	3.436	0.0904
hsa-miR-509-3p	0.0247	0.0937

B

C

D

E

Figure 1.

also increase autophagy flux, when comparing with $EV^{Cx43-KO}$, consistent with a general effect elicited by Cx43-containing EV, regardless of their cellular origin.

Since the regulatory effects of miRNAs can be exerted both on gene expression and on the protein interactions network, we performed a bioinformatic target prediction and protein–protein interaction analysis to uncover the potential biological significance of EV^{Cx43}-enriched miRNAs (Fig 1D). Considering predicted targets that are simultaneously regulated by three or more of the selected miRNAs, we next sought to validate one of these hits - ATP2A2/SERCA2A. Our results demonstrate that the protein levels of ATP2A2/SERCA2A were significantly reduced in cells receiving Cx43-containing EV from either HEK293 or C33a cells, when comparing with cells incubated with EV devoid of Cx43 (Figs 1E and EV3C), corroborating the suitability of our *in silico* approach.

miRNAs enriched in Cx43-containing EV are highly structured

Next, to determine the structural characteristics of the different miRNAs enriched in Cx43-containing EV, we modelled the corresponding 3D structures by applying the RNA Composer algorithm (Popenda *et al*, 2012). The results depicted in Fig 2, show the presence of stable structural elements in some of the miRNAs enriched in Cx43-containing vesicles, comprising double-stranded hairpin loops formed by canonical Watson–Crick base pairings. These elements are clearly defined in the case of miR-133b, miR-410, miR-199a-3p, and miR-744-3p. On the contrary, the miRNAs downregulated in the analyzed Cx43-containing EV show an extended conformation with no apparent secondary structure elements, which would confer a flexible and linear structure to these miRNAs.

miRNA	Structure
hsa-miR-133b E(total) = -437.70 kcal/mol E(VDW) = -309.54 kcal/mol E(elec) = -204.95 kcal/mol	
hsa-miR-410 E(total) = -324.93 kcal/mol E(VDW) = -292.96 kcal/mol E(elec) = -103.16 kcal/mol	
hsa-miR-335-3p E(total) = -345.54 kcal/mol E(VDW) = -226.69 kcal/mol E(elec) = -195.12 kcal/mol	
hsa-let-7d-3p E(total) = -335.75 kcal/mol E(VDW) = -239.88 kcal/mol E(elec) = -176.89 kcal/mol	
hsa-let-7g-5p E(total) = -382.14 kcal/mol E(VDW) = -263.77 kcal/mol E(elec) = -205.11 kcal/mol	
hsa-miR-199a-3p E(total) = -316.71 kcal/mol E(VDW) = -229.26 kcal/mol E(elec) = -179.19 kcal/mol	
hsa-miR-744-3p E(total) = -329.38 kcal/mol E(VDW) = -251.75 kcal/mol E(elec) = -151.95 kcal/mol	

miRNA	Structure
hsa-miR-24-3p E(total) = -331.59 kcal/mol E(VDW) = -257.51 kcal/mol E(elec) = -151.95 kcal/mol	
hsa-miR-454-3p E(total) = -387.23 kcal/mol E(VDW) = -273.90 kcal/mol E(elec) = -191.61 kcal/mol	
hsa-miR-300 E(total) = -301.91 kcal/mol E(VDW) = -248.72 kcal/mol E(elec) = -129.85 kcal/mol	
hsa-miR-509-3p E(total) = -342.26 kcal/mol E(VDW) = -268.56 kcal/mol E(elec) = -254.25 kcal/mol	

Figure 2. miRNAs enriched in Cx43-containing extracellular vesicles are highly structured.

Modelling of the 3D structure of mature miRNAs enriched in both EV^{Cx43+} (red) and EV^{Cx43-} (green). Figure depicts each miRNAs structure, as well as the values of total energy [E(total)], van der Waals energy [E(VDW)] and electrostatic energy [E(elec)].
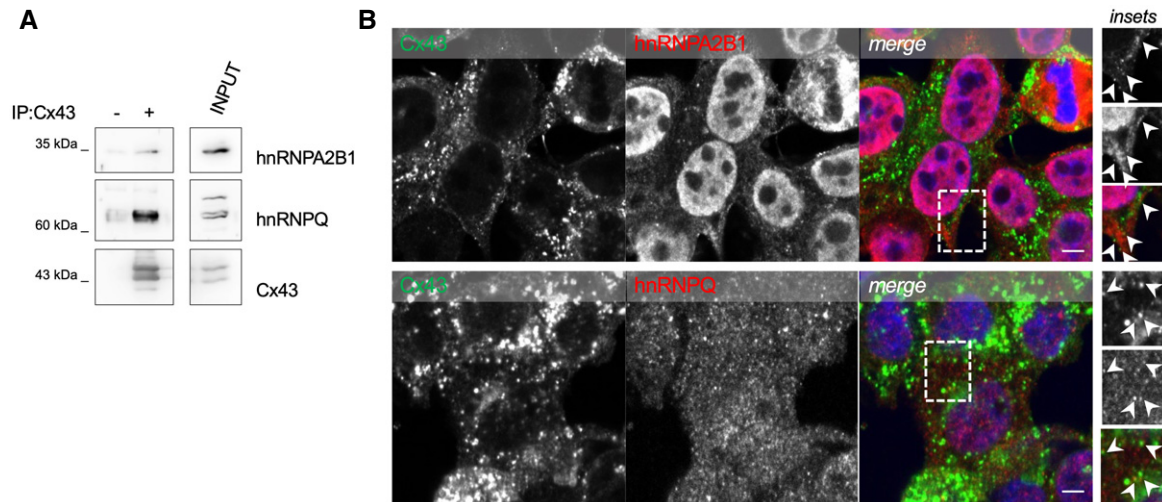
Figure 3. Cx43 interacts with hnRNPA2B1 and hnRNPQ.

A Cx43 was immunoprecipitated (IP) from HEK293^{Cx43+} cells, after which interaction with hnRNPA2B1 and hnRNPQ was analyzed by WB.
B Co-localization between Cx43 (green) and hnRNPA2B1 or hnRNPQ (red) in C33a cells was analyzed by confocal microscopy. Scale bars 10 μm. Arrowheads in the inset images highlight co-localization between Cx43 and hnRNPs.

Source data are available online for this figure.

The levels of miR-133b and miR-199-3p are increased in Cx43-containing EV

Previous studies demonstrated that the RNA binding proteins hnRNPA2B1 and hnRNPQ (also known as SYNCRIP) participate in the selective incorporation of miRNAs in EV, through the recognition of specific miRNAs sequences (Villarroya-Beltri et al, 2013; Santangelo et al, 2016). Grounded on our previous proteomic study unveiling the interaction of Cx43 with multiple hnRNPs in rat hearts, including hnRNPA2B1 and hnRNPQ, we hypothesized that a concerted action between these proteins underlies the selective incorporation of miRNAs in Cx43-containing EV (Martins-Marques et al, 2015a). To address this, we started by evaluating whether Cx43 associates with hnRNPA2B1 and hnRNPQ in HEK293 and C33a cells. Co-immunoprecipitation and fluorescence microscopy assays demonstrate that Cx43 interacted and co-localized with hnRNPA2B1 and hnRNPQ in both cell lines (Figs 3A and B, and EV4A–C).

Next, we validated the miRNAs profiling results by RT-qPCR, by evaluating the levels of three overrepresented miRNAs in Cx43 containing EV—miR-133b, miR-199-3p, and miR-410, and one of the downregulated miRNAs—miR-509-3p, in both cells and EV with or without Cx43. Our results show that miR-133b was significantly upregulated in Cx43-containing EV released by HEK293 and C33a cells, whereas no differences were found in the miR-133b levels in producing cells (Figs 4A and B, and EV5A and E). Cx43-positive EV secreted by C33a cells were also enriched in miR-199-3p, while the levels of miR-410 presented a trend towards an increase, with no differences in EV-producing cells (Fig EV5B, C, F and G). On the other hand, the levels of secreted miR-509-3p were identical in all populations of EV and their corresponding producing cells (Figs 4C and D, and EV5D and H).

We also performed shRNA-mediated knockdown of either hnRNPA2B1 or hnRNPQ (Appendix Fig S1A), after which we evaluated the levels of secreted miRNAs in EV containing or not Cx43. Our results demonstrate that knockdown of either RNA-binding protein did not significantly affect the secretion of miR-133b, miR-199a-3p, miR-410, and miR-509-3p within Cx43-positive EV (Figs 4A and C, and EV5A–D). Nonetheless, there was an increase in the release of miR-133b and miR-199-3p in EV$^{Cx43-KO}$ produced by hnRNPA2B1-knockdown C33a cells (Fig EV5A and B), and a decrease of miR-509-3p in EV^{Cx43-} derived from hnRNPQ-knockdown HEK293 cells (Fig 4C), suggesting that hnRNPs can modulate the selective sorting of EV-miRNAs independently of the presence of Cx43, which may also be cell-type specific.

In addition, we overexpressed GFP-tagged hnRNPA2B1 or hnRNPQ in HEK293^{Cx43+} and HEK293^{Cx43-} cells (Appendix Fig S1B),

Figure 4. The levels of miR-133b are increased in Cx43-containing extracellular vesicles.

A–D EV-producing cells expressing or not Cx43 (HEK293^{Cx43+} or HEK293^{Cx43-}) were transiently transfected with shRNAs targeting hnRNPA2B1, hnRNPQ or non-target shRNAs, for 48 h. miR-133b levels were assessed in EV^{Cx43+} and EV^{Cx43-} (A; n = 6–12 biological replicates) and EV-producing cells (B; n = 4–9 biological replicates). miR-509-3p levels were assessed in EV^{Cx43+} and EV^{Cx43-} (C; n = 6–15 biological replicates) and EV-producing cells (D; n = 4–9 biological replicates).
E–H HEK293^{Cx43+} or HEK293^{Cx43-} were transiently transfected with hnRNPA2B1-GFP, GFP-hnRNPQ or GFP alone, for 24 h. miR-133b levels were assessed in EV^{Cx43+} and EV^{Cx43-} (E; n = 4 biological replicates) and EV-producing cells (F; n = 3 biological replicates). miR-509-3p levels were assessed in EV^{Cx43+} and EV^{Cx43-} (G; n = 4 biological replicates) and EV-producing cells (H; n = 3 biological replicates).

Data information: P-values were derived by Mann–Whitney test. Bars and error bars indicate mean ± SD in all graphs.

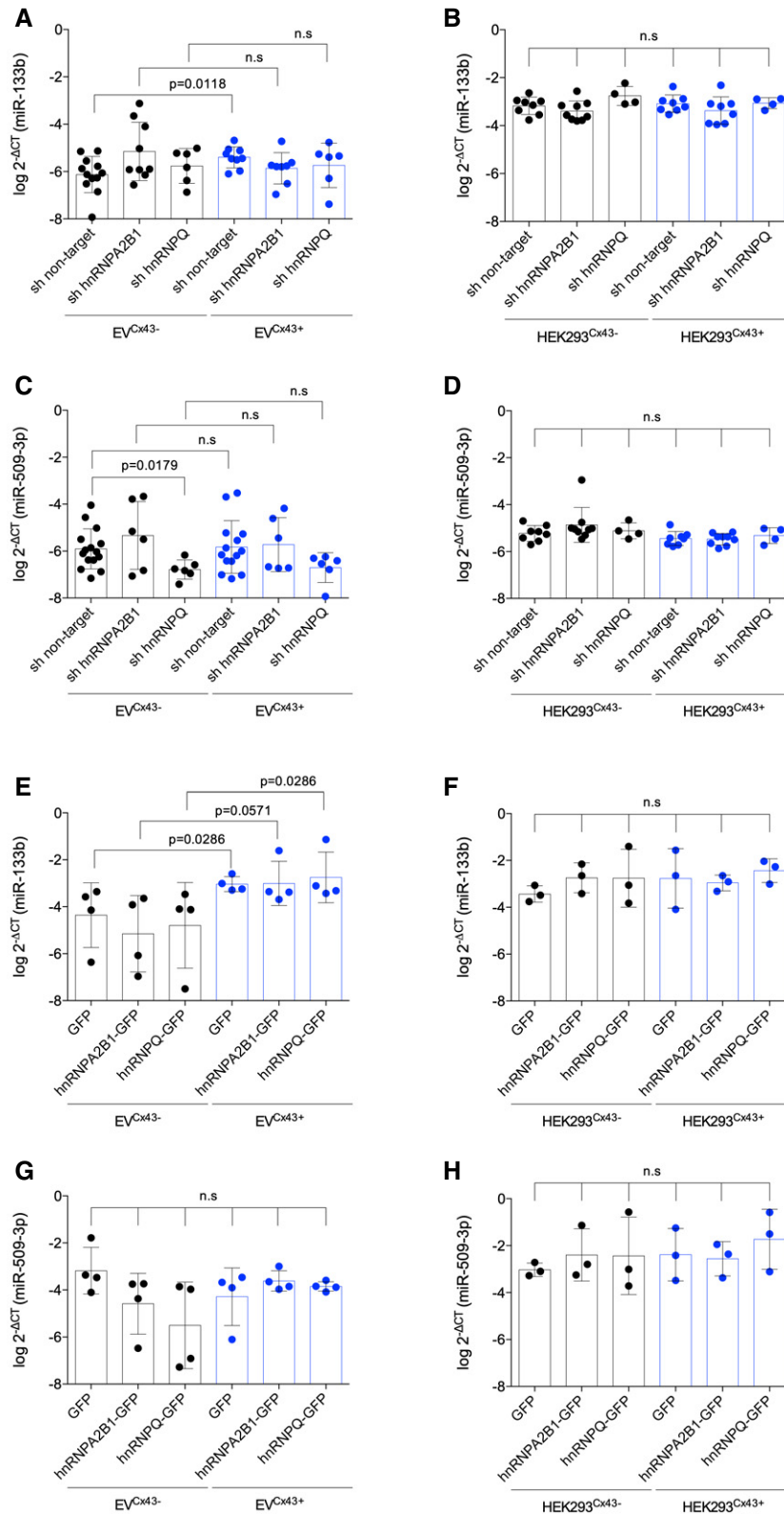**Figure 4.**

followed by the evaluation of the levels of miR-133b and miR-509-3p in EV-producing cells and released vesicles. Results displayed on Fig 4E show that the levels of miR-133b were significantly higher in

EV released by Cx43-containing cells overexpressing either hnRNPA2B1-GFP, GFP-hnRNPQ or GFP alone, when compared with the corresponding EV^{Cx43-}. Nonetheless, the overexpression of

either RNA-binding protein did not further increase the levels of secreted miR-133b in EV^{Cx43+}, suggesting that the presence of Cx43 is determinant for the release of this miRNA. The secretion of miR-509-3p remained unchanged in all experimental conditions (Fig 4G). Similar to what we observed in the knockdown experiments, the levels of miR-133b and miR-509-3p in EV-producing cells were not affected by the overexpression of hnRNPs (Fig 4F and H).

Cx43 participates in selective sorting of miR-133b

Cell-free assays were previously reported as suitable tools to investigate MVB biogenesis and cargo sorting into intraluminal vesicles (ILVs), including synthetic miRNAs (Shurtleff *et al*, 2016). Therefore, we implemented an identical strategy to monitor the role of Cx43 in miRNAs incorporation into vesicles. We started by validating the experimental procedure, monitoring the protection of a luciferase fused to the Cx43 C-terminal, which is facing the intraluminal side of the vesicles during ILV biogenesis (Appendix Fig S2A). For that, we incubated cytosolic fractions of cells devoid of Cx43 with membranes prepared from HEK293^{Cx43-} transiently transfected with Cx43-luciferase in the presence of its membrane-impermeable substrates luciferin and ATP. Next, the reactions were treated with trypsin, to digest non-incorporated luciferase, after which we measured the remaining luciferase activity, derived from Cx43-luciferase that was sequestered into vesicles during the assay (Appendix Fig S2B). Results on Fig 5A show that maximum luciferase protection was achieved by incubation at 30°C, being lost in the presence of TX100, suggesting that our experimental setup is suitable to mimic biogenesis of Cx43-containing vesicles *in vitro*.

To monitor the selective incorporation of miRNAs in Cx43-positive vesicles, we performed incubation of membranes and cytosolic proteins derived from either HEK293^{Cx43+} or HEK293^{Cx43-} cells with an ATP regenerating system, supplemented with synthetic miR-133b or miR-509-3p. After incubation, reactions were either treated or not with RNAse I to digest unpackaged miRNAs, followed by quantification of protected miR-133b or miR-509-3p, by RT-qPCR. Results displayed on Fig 5B demonstrate that the incorporation of miR-133b, but not of miR-509-3p, was higher in reactions performed with membranes and cytosol from Cx43-expressing cells, further corroborating the role of Cx43 in the selective sorting of miR-133b to EV.

To evaluate whether Cx43 can bind to endogenous miR-133b, we next performed UV crosslinking immunoprecipitation (CLIP) in Cx43-expressing cells. Results presented on Fig 5C show that miR-133b was specifically co-immunoprecipitated with Cx43, in contrast with miR-509-3p. In addition, pull-down experiments using cellular extracts and biotinylated miRNAs demonstrate that higher levels of Cx43 were precipitated by biotin-tagged miR-133b, when compared with miR-509-3p (Fig 5D).

To address the involvement of hnRNPA2B1 and hnRNPQ in the interaction between Cx43 and miR-133b, we conducted an electrophoretic mobility shift assay (EMSA) following incubation of *in vitro* translated Cx43 and purified GST-hnRNPA2B1 or GST-hnRNPQ proteins (Appendix Fig S2C and D), with Cy3-tagged miRNAs. Importantly, WB analysis of *in vitro* translated Cx43 demonstrated that higher molecular weight forms of Cx43 could be found in non-reducing conditions (Appendix Fig S2C), suggesting the presence of Cx43 hexameric structures. Our data reveal that Cx43 was able to specifically bind to miR-133b, which could be prevented by an excess of unlabeled competitor (Fig 5E). Interestingly, the presence of hnRNPs created greater shifted bands, suggesting that binding to miR-133b involves a multiprotein complex formed between Cx43 and hnRNPA2B1 or hnRNPQ (Fig 5F). Nonetheless, binding of miR-133b to either hnRNP alone appeared to be stronger than to Cx43 (Fig 5F, comparing lanes 5–6 with lane 2). On the other hand, binding to miR-509-3p also occurred in the presence of the *in vitro* translation machinery alone (Fig 5G and H), likely due to the establishment of non-specific protein-miRNAs interactions.

Based on our *in silico* models, suggesting that Cx43 preferentially binds to highly structured miRNAs, we perform targeted mutagenesis of miR-133b and miR-199-3p to abrogate their secondary structure (Appendix Fig S2E), after which we assessed the interaction between Cx43-enriched membranes (Appendix Fig S2F) and Cy3-tagged mutated miRNAs by EMSA. Results on Fig 5I show that interaction with Cx43 is decreased following mutation of the miR-199-3p secondary structure. In contrast, mutated miR-133b presented increased binding to membranes, regardless of the presence of Cx43, suggesting that mutation of the secondary structure of miR-133b can favor non-specific protein-miRNAs binding (Appendix Fig S2G).

Figure 5.   Cx43 participates in selective sorting of miR-133b.

A   Cell free EV biogenesis was assessed by relative protection of Cx43-luciferase. Reactions were incubated at 4 or 30°C in the presence of membranes derived from HEK293^{Cx43-} transiently transfected with Cx43-luciferase and cytosol from HEK293^{Cx43-} cells, except in the negative control. 1% TX100 was used to disrupt membranes, where indicated ($n = 3$ biological replicates).

B   Crude membranes and cytosol from broken HEK293^{Cx43+} or HEK293^{Cx43-} cells were mixed in an ATP regenerating system, supplemented with synthetic miR-133b or miR-509-3p, as indicated. Graph depicts the indicated miRNAs levels, assessed by RT-qPCR and represented as percent protected after RNAse I digestion of unincorporated miRNAs ($n = 7$–8 biological replicates).

C   Co-immunoprecipitation of endogenous miR-133b and miR-509-3p following UV crosslinking immunoprecipitation (CLIP) of Cx43 ($n = 3$–5 biological replicates).

D   WB analysis for Cx43 in samples derived by miRNAs pulldowns performed with whole lysates of HEK293^{Cx43+} cells and biotinylated miR-133b and miR-509-3p ($n = 5$ biological replicates).

E–H   EMSA was performed using either Cy3-labeled miR-133b (E,F) or miR-509-3p (G,H), and Cx43 produced by *in vitro* translation inserted into lipid nanodiscs, in the presence or absence of recombinant GST-hnRNPA2B1 or GST-hnRNPQ, as indicated. For competition EMSA, an excess of unlabeled miR-133b or miR-509-3p was used (competitor). Empty nanodiscs were used to control unspecific binding.

I   EMSA was performed using either Cy3-labeled wild-type or mutant miR-199a-3p, and Cx43-enriched membranes prepared from C33a parental cells (Cx43$^+$). Cx43$^-$ membranes were used to control unspecific binding.

Data information: *P*-values were derived by Mann–Whitney test. Bars and error bars indicate mean $\pm$ SD in all graphs.
Source data are available online for this figure.
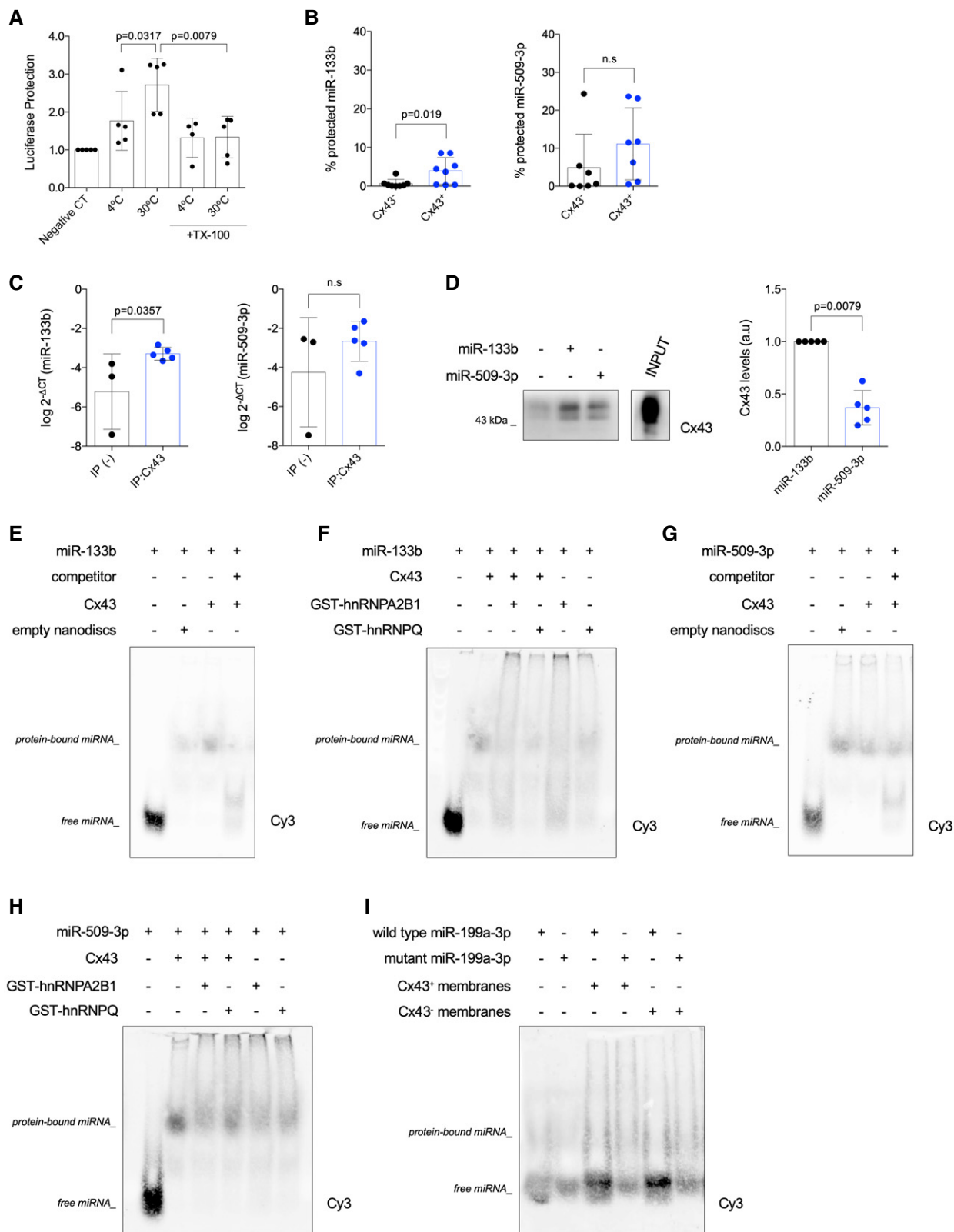
Figure 5.

Next, we sought to address whether the N- (NT) and the C terminus (CT) of Cx43 are the domains involved in Cx43-miRNAs interaction. To assess that, we resorted to a microscopy-based protein-miRNAs binding assay, in which beads were first coated with GST-tagged Cx43 terminals, in the presence or not of GST-hnRNPA2B1 or GST-hnRNPQ, followed by incubation with Cy3-
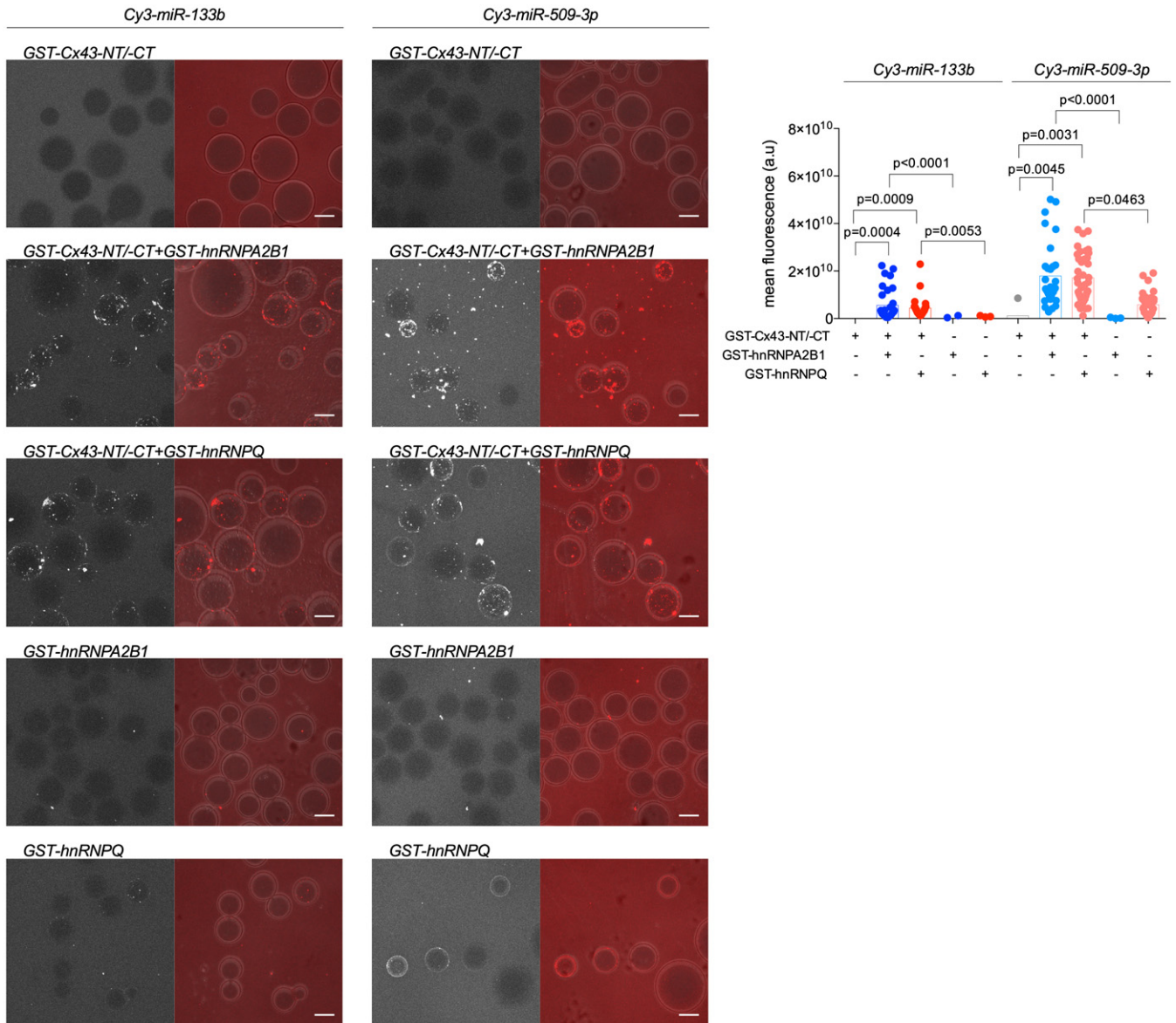
Figure 6. Interaction of Cx43 with miR-133b *in vitro* is increased in the presence of hnRNPA2B1 and hnRNPQ.

Representative maximum projection images of microscopy-based miRNA-protein interaction using beads coated with GST-tagged NT/CT-Cx43, hnRNPA2B1 or hnRNPQ, as indicated, following the addition of Cy3-labelled miR-133b or miR-509-3p. Graph depicts quantification of total fluorescence/bead, as a measure of protein-miRNAs binding. Scale bars 50 μm (*n* = 2 biological replicates; average of 23 beads analyzed/condition).

Data information: *P*-values were derived by Kruskal–Wallis (Dunn's post hoc) test. Bars and error bars indicate mean ± SD in all graphs.

Source data are available online for this figure.

labelled miRNAs. GST alone was used as negative control (Appendix Fig S2H and I). The fluorescence intensity formed around the beads reflects the interaction between the proteins and either miR-133b or miR-509-3p. Representative images displayed in Fig 6 show a strong interaction in the presence of both Cx43 and one of the hnRNPs, regardless of the miRNA, suggesting that both proteins are required for an efficient miRNAs binding. In agreement, miRNAs binding was virtually absent when beads were coated either with Cx43 terminals or with GST-hnRNPA2B1 alone. A weak interaction was detected when GST-hnRNPQ-coated beads

were incubated with miR-509-3p, reinforcing the role of hnRNPQ in binding to miR-509-3p suggested by our RT-qPCR data.

Cx43 facilitates the delivery of intraluminal RNAs to target cells

Results from our laboratory have previously demonstrated that the presence of Cx43 facilitates the release of intraluminal EV cargo into target cells (Soares *et al*, 2015). The results obtained up to this point strongly support a role for Cx43 on the selective sorting of miRNAs to be released in EV. However, it remains to be established whether
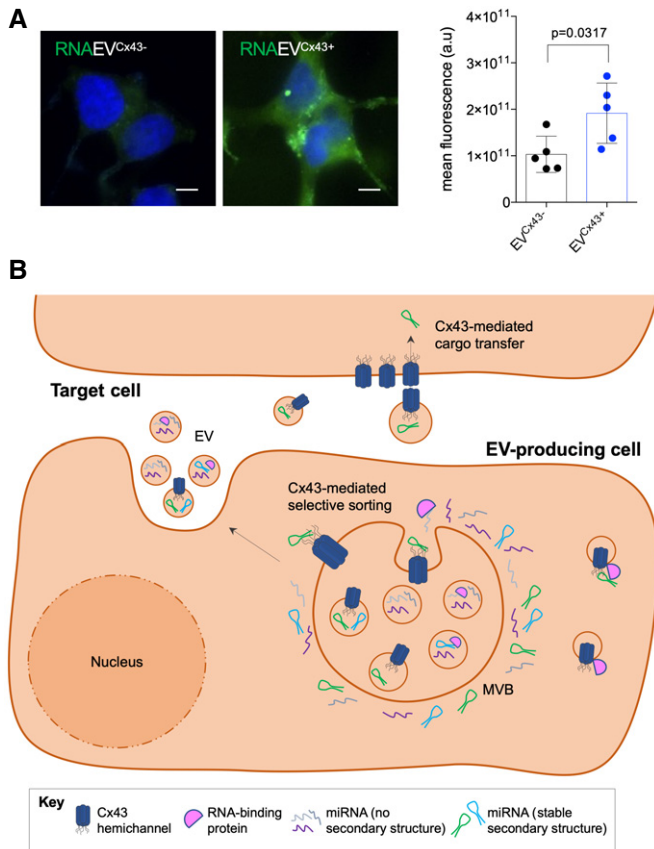
Figure 7. Cx43 facilitates the delivery of intraluminal RNAs to target cells.

A Equal amounts of EV^{Cx43+} and EV^{Cx43-} labelled with SYTO® RNASelect™ green fluorescent stain were incubated with HEK293^{Cx43+} cells for 30 min, at 37°C. Scale bars 10 μm (n = 5 biological replicates). P-values were derived by Mann-Whitney test.

B Working model for the role of Cx43 in mediating the selective sorting of miRNAs into EV. Cx43 preferentially binds to miRNAs harboring a stable secondary structure, mediating its selective incorporation into EV. Although hnRNPs do not seem to directly participate in Cx43-dependent loading of EV-miRNAs, they strength the binding of miRNAs to cx43, suggesting that a multiprotein complex formed between RNA-binding proteins and Cx43 is important to select miRNAs.

EV-Cx43 channels are also important to mediate the delivery of RNA cargo to recipient cells. To address this, we loaded EV^{Cx43+} or EV^{Cx43-} with a fluorescent dye that labels total RNA, after which labelled EV were incubated with HEK293^{Cx43+}. Results depicted on Fig 7A show that EV^{Cx43+} were more efficient in delivering RNAs to target cells, compared to EV^{Cx43-}, reinforcing the concept of Cx43 in modulating the communication between EV and target cells, not only through the selectively incorporation of EV cargo but also facilitating the release of intraluminal contents via Cx43 channels.

Discussion

Multiple lines of evidence have demonstrated that the biological functions of Cx43 go far beyond the canonical role on GJ-mediated communication between adjacent cells. In agreement, Cx43 was

shown to participate in the regulation of gene transcription, ion channel trafficking and mitochondrial homeostasis (Martins-Marques *et al*, 2019). Groundbreaking studies from our lab demonstrated for the first time that Cx43 also plays a role in EV-mediated long-distance communication (Soares *et al*, 2015). In the present work, we provide further evidence supporting that Cx43 mediates the selective sorting of miRNAs into EV, which may involve a direct binding of Cx43 to specific miRNAs, or a concerted action with RNA-binding proteins (working model in Fig 7B).

The results gathered in the present manuscript show that expression of Cx43 in EV-producing cells modulates the profile of secreted miRNAs. Considering that EV-enclosed miRNAs can elicit biological responses in target cells, it is conceivable that the Cx43-dependent miRNAs signature of EV will impact on the phenotype and behavior of receiving cells. Our bioinformatic analysis supports a role for EV^{Cx43+}-enriched miRNAs in multiple signaling pathways and biological processes, including circadian rhythm and autophagy. In agreement, our results are consistent with a role for Cx43-containing EV in increasing autophagy flux. The role of EV-enclosed miRNAs upon modulation of autophagy is not without precedents. In fact, it was previously shown that vesicular miR-210 leads to autophagy suppression in lung fibroblasts, contributing to the pathophysiology of chronic obstructive pulmonary disease (Fujita *et al*, 2015), while macrophage EV enriched in miR-421-3p can activate autophagy, which was proposed as a potential therapeutic strategy for spinal cord injury (Wang *et al*, 2020). Although further studies are required to better understand the biological implications of the miRNAs landscape of EV^{Cx43+}, our results also confirm that Cx43-containing vesicles modulate the levels of ATP2A2/SERCA2A in target cells, likely impacting on Ca^{2+} homeostasis. Since increased cytosolic Ca^{2+} concentrations have been associated with stimulation of autophagy, it is plausible that decreased levels of ATP2A2/SERCA2A in cells treated with Cx43-containing EV may also contribute to promote autophagy flux in those cells.

Although our first analysis by high-throughput low-density arrays performed in HEK293 cells showed decreased levels of miR-509-3p within EV^{Cx43+}, validation of this individual hit by RT-qPCR revealed similar amounts in EV containing or not Cx43, likely as a result of the increased signal-to-noise ratio obtained in single RT-qPCR experiments. Furthermore, experiments on EV derived from C33a cells confirmed that the presence of Cx43 did not impact the release of miR-509-3p. In contrast, we provide compelling evidence that secretion of miR-133b and miR-199a-3p were increased in Cx43-containing EV, which was not affected by genetic manipulation of either hnRNPA2B1 or hnRNPQ. Several explanations may be attempted, including an upstream role of Cx43 in the selective sorting mechanism of miR-133b and miR-199a-3p that may not be shared by other miRNAs, the presence of active amounts of RNPs after silencing, or redundant roles played by other RNA-binding proteins. In fact, multiple proteins have been associated with selective sorting of EV-miRNAs, including YBX-1, MVP, HuR, MEX3C, Lupus La, Alyref, and Fus. While proteomic studies from our lab have previously identified the interaction between Cx43 and MVP, it is currently unclear whether Cx43 can also interact with the other RNA-binding proteins associated with EV-miRNAs incorporation and if so, what could be the downstream effect of those protein–protein interactions (Martins-Marques *et al*, 2015a). Surprisingly, knockdown of hnRNPA2B1 in C33a cells increased the secretion of

miR-133b and miR-199-3p in EV devoid of Cx43, while hnRNPQ knockdown in HEK293 cells decreased the release of miR-509-3p in EV without Cx43, implicating these RNA-binding proteins in the sorting of miRNAs in the absence of Cx43, an effect that also appears to be cell-type specific. In agreement, recent studies demonstrated that miRNAs secretion is a highly complex mechanism involving the recognition of multiple sequence codes for EV release and cellular retention, with the participation of various RNA-binding proteins in a cell-type-specific manner (Garcia-Martin *et al*, 2022). Being cells from different origins—HEK293 is an embryonic kidney cell line, while C33 is a tumor epithelial cell line—it is likely that both biological functions and signals that govern miR-133b secretion are different. For example, miR-133b acts as a tumor suppressor in various cancers, including endometrial carcinoma, being its levels diminished in tumor cells-derived EV (Cai *et al*, 2020; Liao *et al*, 2021). On the other hand, an increase of miR-133b is implicated in renal disease (Sun *et al*, 2018). Despite being conceivable that in the absence of both hnRNPA2B1/hnRNPQ and Cx43 other compensatory mechanisms are activated to mediate the selective sorting of EV-miRNA, further investigation is required to better characterize possible synergistic and/or competition effects.

Previous reports have identified that the miRNAs motifs for recognition by hnRNPA2B1 and hnRNPQ are different (Villarroya-Beltri *et al*, 2013; Santangelo *et al*, 2016). Given that the miR-133b sequence contains both motifs (GGAG and GGCU), competition between these two RNA-binding proteins may also occur, ultimately modulating EV cargo sorting. Our experimental evidences could also be supported by the recent description of non-canonical functions of some miRNAs, different from the negative post-transcriptional regulation of coding genes (Yang *et al*, 2021). Belter and coworkers identified the presence of putative secondary structure elements in some mature miRNAs sequences, which suggested their involvement in aptamer-like interactions with proteins in other biological scenarios (Belter *et al*, 2014). The existence of stable secondary structure elements in the miRNAs enriched in Cx43-containing vesicles can also contribute to their specific sorting, which was reinforced by our data showing a decreased binding of Cx43 to a mutated miR-199-3p with no secondary structure.

Our results using either CLIP in intact cells or pull-down experiments demonstrate that Cx43 co-precipitates with miR-133b, which was not observed with miR-509-3p. However, the use of cellular extracts, rather than purified proteins, cannot guarantee that Cx43 directly interacts with miR-133b, being conceivable that RNA-binding proteins bridge the association of Cx43 to miRNAs. In agreement, it was previously described that interaction between the lysosomal membrane protein Lamp2c and hnRNPA1 mediates the selective Lamp2c-dependent import of RNA into lysosomes (Fujiwara *et al*, 2013).

Our EMSA experiments demonstrate that binding of Cx43 to miR-133b can occur in the absence of hnRNPs, despite a multiprotein complex between Cx43 and hnRNPA2B1 or hnRNPQ increasing the binding to miR-133b. Importantly, binding of miR-133b to either hnRNPA2B1 or hnRNPQ in the absence of Cx43 was stronger when compared with Cx43 alone. Although these *in vitro* studies, resorting to purified proteins and nucleic acids, are vital to ascertain direct protein-RNA binding, they do not recapitulate the cellular milieu, where other miRNAs and proteins also exist and may compete for common binding sites. In fact, while our *in vitro* data demonstrate

that the presence of Cx43 together with hnRNPA2B1/hnRNPQ strengthens miRNAs binding, it does not translate into decreased EV-miR-133b secreted by cultured cells, where both RNA-binding proteins appear to be dispensable for selective sorting of miRNAs by Cx43.

Surprisingly, when we used the purified NT/CT of Cx43, binding to miR-133b only occurred when at least one hnRNP was present, similarly to what is observed with miR-509-3p. Although previous *in silico* analysis have uncovered several RNA-binding motifs in the Cx43 sequence, namely in the CT and NT domains, additional motifs can be found in the extracellular and intracellular loops of the protein (Varela-Eirin *et al*, 2017). Since in this experimental setup, binding selectivity to miR-133b over miR-509-3p was lost, it is likely that (i) selectivity of miR-133b binding to Cx43 is conferred by a different region within the protein, namely the intracellular loops, (ii) the 3D-arrangement of the Cx43 channel, which cannot be recapitulated in this assay, is required to confer selectivity for miR-133b, and/or (iii) selectivity of miR binding to Cx43 requires other proteins that are absent in this *in vitro* assay.

Sumoylation and hyperoxia-induced *O*-GlcNAc glycosylation of hnRNPA2B1 were previously identified as important signals driving specific miRNAs recognition and secretion (Villarroya-Beltri *et al*, 2013; Lee *et al*, 2019). Considering that many post-translational modifications (PTMs) can occur in response to distinct environmental cues, the role of Cx43 and hnRNPs upon EV-miRNAs sorting may change under different pathophysiological conditions. Cx43 can also be modified by a wide variety of PTMs, including phosphorylation, ubiquitination, and sumoylation, which have been related with the modulation of Cx43 channel function, interactome, as well as with the release of Cx43 into EV (Martins-Marques *et al*, 2020a, 2020b). We can also speculate that PTMs on Cx43 may affect its binding to miRNAs and/or to hnRNPs, thus changing EV content, analogously to what has been described for the caveolin-1/hnRNPA2B1 interaction (Lee *et al*, 2019). Our previous proteomic data demonstrated that heart ischemia and reperfusion modulate the interaction between Cx43 and hnRNPA2B1 and hnRNPQ (Martins-Marques *et al*, 2015a). In these conditions, we also demonstrated that the release of Cx43 into EV was impaired (Martins-Marques *et al*, 2020b). Nevertheless, it remains to be established whether ischemia-induced changes on Cx43 impact on the sorting of miRNAs into EV is dependent or not of the association with different hnRNPs. Considering the effects of Cx43-enriched EV-miRNAs upon Ca^{2+} signaling and autophagy in target cells, and the well-established implications of these mechanisms in multiple human diseases, including cardiac and neurodegenerative disorders such and Alzheimer's, Huntington's, and Parkinson's disease, it is conceivable that disease-associated changes in the selective sorting process result in a distinct profile of miRNAs secreted by unhealthy cells, which, in turn, may significantly impact homeostasis, function and behavior of target cells, thus contributing to disease spreading and progression and/or mount an orchestrated repair approach. On the other hand, the miRNA landscape of EV found in biological fluids may also reflect Cx43-dependent miRNAs sorting under pathological conditions, thus providing a clue about the disease-associated mechanisms and opening the door for Cx43-targeted therapies.

In addition to selective incorporation of miRNAs in EV, it is tempting to speculate that changes in the Cx43 interactome under

pathological conditions impact on the sorting of proteins to be secreted, similar to what is described for the tetraspanin CD81, which depletion impaired the release of CD81-interacting partners, including ionic channels and Ras-related proteins (Perez-Hernandez *et al*, 2013). Nonetheless, further studies are required to investigate the role of Cx43 in protein sorting into EV.

Altogether, our work unveiled a novel biological role for Cx43 upon the selective sorting of miRNAs into EV, which may have important implications for long-distance cell–cell communication in health and disease.

Materials and Methods

Antibodies and chemicals

Antibodies against Calnexin (AB0041), CD63 (AB0047), Cx43 (AB0016), GAPDH (AB0049), GFP (AB0020) and GST (AB99919) were obtained from SICGEN (Cantanhede, Portugal), and against Flotillin-1 (sc-25506), CD81 (H-121, sc-9158), hnRNPA2B1 (sc-374053) and hnRNPQ (I8E4, sc-56703) were from SCBT (Heidelberg, Germany). Antibodies against Tsg101 (4A10, GTX70255) were obtained from Gentex (Zeeland, MI, USA), against turboGFP (PA5-22688) and LC3 (PA116931) were from Thermo Fisher Scientific (Waltham, MA, USA), against ATP2A2/SERCA2 (4388S) were from Cell Signaling Technology (Danvers, MA, USA). Unless stated otherwise, all chemicals were obtained from Sigma-Aldrich (St. Louis, MO, USA).

Cell cultures

Human embryonic kidney (HEK)-293 and C33a cells were cultured in Dulbecco's modified Eagle medium (DMEM, Gibco), supplemented with 10% FBS (Gibco, Thermo Fisher Scientific) and Penicillin/Streptomycin (100 U/ml: 100 µg/ml), at 37°C under 5% CO_2. HEK293^{Cx43+} cell line was established as previously described (Catarino *et al*, 2011). Briefly, HEK293 parental cells (HEK293^{Cx43-}) were transduced with the lentiviral vector pLenti6-prom-CMV-V5-C1-Cx43. After 1 day, 8 µg/ml blasticidin was added to select transduced cells. Knockout (KO) of Cx43 in parental C33a cells was generated using our previously described protocol (Tishchenko *et al*, 2020).

siRNA-mediated knockdown

Protein knockdown was achieved by general transfection after cells reached 50–60% confluence. For transfection of 3×10^6 HEK293 cells, 3.5 µg shRNA was complexed with Lipofectamine™ 2000 (Thermo Fisher Scientific), while 3×10^6 C33a cells were transfected with 5.6 µg shRNA complexed with Lipofectamine™ 3000 (Thermo Fisher Scientific), according to the manufacturer's recommendations. Experiments were performed 48 h after transfection. shRNA targeting hnRNPA2B1 (Mission shRNA, TRCN0000001059; target sequence: CAGAAATACCATACCATCAAT) and hnRNPQ (Mission shRNA, TRCN0000275206; target sequence: GTATGAC-GATTACTACTATTA) were purchased from Sigma-Aldrich. Non-targeting scrambled sequences (Sigma-Aldrich) were used as controls.

Plasmid constructions and cell transfection

Plasmids expressing Cx43-luciferase were generated by cloning the appropriate luciferase cDNA into a pcDNA ENTR BP vector containing Cx43. Plasmids expressing GFP-hnRNPQ were generated by cloning the appropriate hnRNPQ cDNA into a custom pcDNA ENTR BP GFP C2 vector. Plasmid encoding for hnRNPA2B1-GFP (turboGFP) was kindly provided by Dr Francisco Sanchez Madrid (Villarroya-Beltri *et al*, 2013). Transient transfection of cells was performed with Lipofectamine™ 2000, according to the manufacturer. Experiments were performed 24 h after transfection.

EV isolation from cultured cells

EV-depleted medium was prepared by ultracentrifugation of 50% FBS in the appropriate cell culture medium (120,000 *g*, 16 h) (Théry *et al*, 2006; Soares *et al*, 2015). EV derived from cultured cells were isolated from conditioned medium after culture in EV-depleted medium. Harvested supernatants were subjected to differential centrifugation at 4°C, starting with 300 *g*, for 10 min, followed by 16,500 *g*, for 20 min. Supernatants were filtered (0.22 µm filter units, cellulose acetate) and ultracentrifuged at 120,000 *g*, for 70 min. EV pellets were resuspended in PBS. EV were characterized by transmission electron microscopy (TEM) and nanoparticle tracking analysis (NTA).

miRNAs profiling and *in silico* functional analysis

Total RNA was extracted from purified EV using miRNeasy Serum/Plasma Advanced Kit (Qiagen, Hilden, Germany), followed by quality assessment using microfluidics chips to ensure rRNA contamination level < 0.5% (Agilent, Bioanalyzer, RNA nano-chip). miRNAs expression profiling of exosomes was evaluated by high-throughput low-density arrays, based on real-time (RT)-PCR, using the Exiqon miRCURY™ LNA system (Exiqon, Denmark). Data from quantitative RT-PCR (RT-qPCR) were analyzed by the Delta-Ct method with the DataAssist software (Thermo Fisher Scientific). Adjusted *P*-values between sample groups were calculated by using Benjamin Hochberg False Discovery Rate (FDR). miRNA-regulatory relationships were determined using mirDIP algorithm (Tokar *et al*, 2018) and the enrichment analysis was performed with Enrichr (Kuleshov *et al*, 2016). Protein–protein interactions were obtained from STRING database (Szklarczyk *et al*, 2019).

Mature miRNAs structure modelling

Selected sequences of the analyzed mature miRNAs were extracted from the miRbase database v.22.1 (Kozomara & Griffiths-Jones, 2014). All the sequences were submitted to 3D structure modelling by the Composer algorithm (Popenda *et al*, 2012). This algorithm is designed as a pipeline that combines a the CentroidFold secondary structure prediction algorithm (Sato *et al*, 2009), together with the extraction of RNA tertiary structure elements from the FRABASE database (Popenda *et al*, 2010) and the generation of the corresponding 3D model in PDB format. All the obtained structures were represented with the help of the Protein Imager software (Tomasello *et al*, 2020).

Western Blot (WB) analysis

In experiments where non-reducing conditions were required, β-mercaptoethanol was omitted from the classical Laemmli buffer used to denature the samples. Samples were separated by sodium dodecyl sulfate/polyacrylamide gel electrophoresis (SDS-PAGE) and transferred to nitrocellulose membranes (Bio-Rad, Hercules, CA, USA). Membranes were blocked with 5% non-fat milk in Tris-buffered saline-Tween 20 (TBS-T; 20 mM Tris, 150 mM NaCl, 0.2% Tween 20, pH 7.6), probed with appropriate primary antibodies and horseradish peroxidase (HRP)-conjugated secondary antibodies. Proteins of interest were visualized by chemiluminescence using a VersaDoc system (Bio-Rad). Densitometric quantification was performed in unsaturated images using ImageJ (National Institutes of Health, Bethesda, MD, USA).

Transmission electron microscopy (TEM)

EV and lipid nanodiscs were fixed with 2% PFA and deposited on Formvar-carbon coated grids (TAAB Laboratories Equipment, Berks, UK). Samples were washed with PBS and fixed with 1% glutaraldehyde for 5 min. Grids were washed with water, contrasted with an uranyl-oxalate solution pH 7, for 5 min, and transferred to methyl-cellulose—uranyl acetate for 10 min on ice, as previously described (Soares *et al*, 2015; Martins-Marques *et al*, 2016). Images were collected using a Tecnai G2 Spirit BioTWIN electron microscope (FEI, Oregon, USA) at 80kV.

Nanoparticle tracking analysis (NTA)

EV were resuspended in 1 ml of PBS, after which NTA was performed using NanoSight LM 10 instrument (NanoSight Ltd, Malvern, United Kingdom). Analysis settings were optimized and kept constant between samples and each video was analyzed to give the mean size and estimated concentration of particles. Data were processed using NTA 2.2 analytical software (NanoSight Ltd).

Immunoprecipitation (IP)

Cell lysates were prepared in RIPA buffer, containing protease inhibitors (protease inhibitor cocktail (Roche), 2 mM PMSF, 10 mM iodoacetamide, 2 mM sodium orthovanadate). IP were performed in 500 μg total protein lysates by incubation with the appropriate primary antibodies (0.5 μg goat anti-Cx43, AB0016, Sicgen; 0.5 μg mouse anti-hnRNPA2B1, sc-374053, SCBT; 1.0 μg mouse anti-hnRNPQ, I8E4, sc-56703, SCBT) overnight, at 4°C under agitation. Protein G Sepharose beads (GE Healthcare, Chicago, IL, USA) were added and incubated for 1.5 h, at 4°C, followed by washing in RIPA buffer. Complexes were eluted in Laemmli buffer and denatured at 95°C, for 5 min before WB analysis.

Fluorescence microscopy and immunostaining

Cells grown on fibronectin-coated coverslips were fixed in 4% PFA for 10 min and permeabilized with 0.2% TX100 for 10 min. Specimens were blocked with 2.5% BSA for 20 min, followed by incubation with appropriate primary antibodies overnight, at 4°C. Alexa Fluor-conjugated secondary antibodies (Thermo Fisher Scientific)

were incubated for 1 h, at room temperature. All solutions were made in 0.25% BSA. Nuclei were stained with DAPI. Specimens were mounted with Mowiol 4-88 (Sigma-Aldrich). For controls, primary antibodies were omitted. Images were analyzed by confocal microscopy in a Zeiss LSM 710 (Carl Zeiss AG, Jena, Germany) with a Plan-Apochromat 63×/1.4 Oil DIC M27 objective (Carl Zeiss AG). For monitoring of autophagy, HEK293 cells transfected with GFP-LC3 were treated with 5 μg of either EV^{Cx43+} or EV^{Cx43-} for 24 h. Cells were serum-starved for 6 h, before fixation in 4% PFA and nuclei staining with DAPI. Microscopy images were obtained using an Axio Observer.Z1 inverted microscope (Carl Zeiss AG) with a Plan-Apochromat 63×/1.4 Oil DIC M27 objective (Carl Zeiss AG). The number of GFP-LC3 punctated dots per cell (average of 30 cells/independent experiment) was quantified using ImageJ.

UV crosslinking immunoprecipitation (CLIP)

Cell monolayers were subjected to UV crosslinking (400 mJ/cm^2), followed by cell lysis (0.1% SDS, 0.5% sodium deoxycholate (DOC), 0.5% NP-40 in PBS) containing 50 U/ml RNAse inhibitor (NZYtech) and protease inhibitor cocktail (Roche). IP of Cx43 was performed after dilution in IP buffer (1 mM EDTA pH 8.0, 0.5 mM EGTA pH 8.0, 10 mM Tris-HCl pH 8.0, 1% Triton X-100, 0.1% DOC, containing 50 U/ml RNAse inhibitor and protease inhibitor cocktail) by incubation with the primary antibody (goat anti-Cx43, AB0016, Sicgen) overnight, at 4°C under agitation. IP controls were performed by incubation with goat anti-GFP antibodies (AB0020, Sicgen). 10% of the lysate samples were kept for normalizing IP fractions in the RT-qPCR assay. Protein G Sepharose beads (GE Healthcare) were added and incubated for 2 h, at 4°C, followed by sequential washing with low salt buffer (0.1% SDS, 1% Triton X-100, 2 mM EDTA, 20 mM Tris-HCl pH 8.0, 150 mM NaCl), high salt buffer (0.1% SDS, 1% Triton X-100, 2 mM EDTA, 20 mM Tris-HCl pH 8.0, 500 mM NaCl) and LiCl salt buffer (0.25 M LiCl, 1% DOC, 1% NP-40, 1 mM EDTA, 10 mM Tris-HCl pH 8.0). Complexes were eluted (10 mM Tris-HCl pH 8.0, 1 mM EDTA pH 8.0, 1% SDS and 50 U/ml RNAse inhibitor), under heating at 65°C, followed by treatment with 1.2 mg/ml Proteinase K (Thermo Fisher Scientific) for 2 h, at 50°C. RNA was extracted by phenol:chloroform:isoamyl alcohol (Sigma-Aldrich) before RT-qPCR analysis.

Quantification of miRNAs by RT-qPCR

Total RNA was isolated from EV using miRNeasy Serum/Plasma Advanced Kit (Qiagen) and from cellular extracts using NZYol (nzytech, Lisboa, Portugal). cDNA synthesis was performed with the Universal miRCURY LNA^{TM} cDNA synthesis kit (Exiqon), following manufacturer's instructions. Quantification of selected miRNAs by RT-qPCR was performed with specific LNA primers (miRCURY LNA miRNA PCR Assays, Qiagen). Expression levels of miR-133b, miR-199-3p, miR-410, and miR-509-3p are represented as $\log^{2-\Delta Ct}$, using the U6 snRNA levels as reference.

Production of recombinant proteins

Glutathione S-transferase (GST), GST-hnRNPA2B1, GST-hnRNPQ and GST-Cx43 N-terminal (GST-Cx43 NT) and GST-Cx43 C-Terminal (GST-Cx43 CT) were generated by cloning the

appropriate cDNA into pGEX4T1 vectors. Recombinant proteins were expressed in *Escherichia coli* BL21 (Thermo Fisher Scientific), induced by 0.1 mM isopropyl β-D-1-thiogalactopyranoside (IPTG), overnight at 20°C. GST-fusion proteins were purified using GSTrap™ high-performance columns (GE Healthcare). GST-hnRNPA2B1 was further purified by size exclusion chromatography (Superdex™ 200, GE Healthcare), whereas GST-hnRNPQ was further purified by ionic exchange chromatography (Mono S™, GE Healthcare). Cell-free synthesis of full-length Cx43 was performed using the MembraneMax™ protein expression system (Thermo Fisher Scientific), according to manufacturer's instructions.

Cell-free packaging assay

Preparation of cytosol and membrane extracts

HEK293^{Cx43-} or HEK293^{Cx43+} cellular extracts were resuspended in homogenization buffer (250 mM sorbitol, 137 mM NaCl, 5 mM Tris-HCl, pH 7.4, supplemented with protease and phosphatase inhibitors) and passed 15–20 times through a 23-gauge needle until disruption of > 80% of the cells, as assessed by microscopy (Shurtleff *et al*, 2016). On average, 4 µg/µl cytosolic fractions were obtained from 6×10^6 HEK293 cells. Cell debris were discarded after centrifugation at 1,500 *g* for 5 min. Supernatants were centrifuged at 15,000 *g* for 20 min, followed by 16,100 *g* for 30 min to generate the cytosolic fraction (supernatant). Membrane pellet was resuspended in homogenization buffer supplemented with 1 M LiCl, followed by centrifugation at 16,100 *g* for 30 min, to generate the membrane fraction (pellet).

Cell-free biogenesis assay

Membranes were prepared from HEK293^{Cx43-} transiently transfected with Cx43-luciferase and cytosol was prepared from HEK293^{Cx43-} cells. Biogenesis reactions consisted of 2 µg/µl (final concentration) of cytosolic fraction, combined with 0.65 µg/µl (final concentration) of membranes in incorporation buffer (16 mM KCl, 4 mM CaCl$_2$, 300 µM MgOAc, 200 µM DTT, 2.5 mM HEPES pH 7.4) and an ATP regeneration system (10 mM ATP, 2 mM creatine phosphate, 50 µg/ml creatine phosphokinase, 10 mM MgCl$_2$). Reactions were incubated for 20 min at 30°C, after which membranes were pelleted at 15,000 *g* for 10 min, at 4°C, and resuspended in 0.5 mg/ml trypsin (in PBS). Incubations proceeded for 1 h at 4°C to induce cleavage of non-internalized Cx43-luciferase. Luciferase activity was measured in opaque 96-well plates, after incubation for 2 min at room temperature, using a Biotek Synergy HT microplate reader, analyzed with the Gen 5 software (Biotek). Luciferase activity protection was used as a measure of vesicle biogenesis, calculated as the relative ratio of relative light units compared with a negative control reaction (without cytosol, at 4°C in the presence of 1% TX100).

Cell-free miRNAs packaging assay

2 µg/µl (final concentration) of cytosolic fraction were combined with 0.65 µg/µl (final concentration) of membranes in incorporation buffer and an ATP regeneration system, as described above. Where indicated, 1 µM synthetic miR-133b or miR-509-3p (Sigma-Aldrich) were added to the reaction mix and incubated for 30 min at 30°C.

Reactions were placed on ice, followed by an additional incubation with 10 µg RNAse I (Sigma-Aldrich) for 20 min at 30°C to degrade non-incorporated miRNAs. RNAse I was omitted in the "no RNase" control samples. Reactions were immediately stopped by the addition of NZYol, followed by RNA extraction before RT-qPCR. Percent protection was calculated comparing the Ct of the indicated miRNAs in the RNase-treated samples with the "no RNase" control reaction ($2^{-(Ct_{experimental}-Ct_{control})}$), with the "no RNase" control set to 100%.

miRNAs pull-down

Biotin-labelling of synthetic miR-133b (UUUGGUCCCCUUCAAC-CAGCUA) and miR-509-3p (UGAUUGGUACGUCUGUGGGUAG) was performed using Pierce™ Biotin 3′ End DNA Labeling Kit (Thermo Fisher Scientific), according to manufacturer's instructions. 3×10^6 HEK293^{Cx43+} cells were lysed in RIPA buffer, containing protease inhibitors (protease inhibitor cocktail, 2 mM PMSF, 10 mM iodoacetamide and 2 mM sodium orthovanadate), followed by centrifugation at 1,000 *g* for 5 min. Supernatants were pre-cleared by incubation with 15 µl neutravidin beads for 1 h, at 4°C. Cleared lysates were diluted in TBS-T supplemented with 1 mM EDTA. Incubation with 0.1 µg biotinylated miR-133b or miR-509-3p, where indicated, proceeded for 1 h, at 4°C. Pull-down of biotinylated complexes was performed on neutravidin beads for 1 h, at 4°C. Beads were washed with TBS-T and final pellets resuspended in Laemmli buffer and denatured at 95°C, for 5 min before WB analysis.

Electrophoretic mobility shift assay (EMSA)

5 pmol Cy3-labelled miRNAs (wild-type miR-133b, sequence: UUUGGUCCCCUUCAACCAGCUA; mutant miR-133b, sequence: UUU**C**GUCCCCUUCAACCAGCUA; wild-type miR-509-3p, sequence: UGAUUGGUACGUCUGUGGGUAG; wild-type miR-199-3p, sequence: ACAGUAGUCUGCACAUUGGUUA; mutant miR-199-3p, sequence: A**U**AGUAGUCUGCACAUUGGUUA, Eurofins Scientific, Luxembourg) were incubated with 2 µg purified GST-hnRNPA2B1, GST-hnRNPQ, *in vitro* translated Cx43 and/or 10 µg of membrane extracts prepared from C33a parental or Cx43-knockout cells, as detailed in the "cell-free biogenesis assay" section. Binding reactions were performed in EMSA binding buffer (10 mM Tris-HCl pH 7.5, 1 mM EDTA, 100 mM KCl, 5% glycerol, 0.01 mg/ml BSA), for 1 h at 30°C. For competition EMSA, 100 pmol of unlabeled miRNAs were used. Binding reactions were run in a 10% polyacrylamide gel for 1 h at 10 V/cm^2, followed by transfer to nylon membranes and fluorescence detection in a Typhoon™ laser-scanner platform (GE Healthcare) (Hellman & Fried, 2007).

Microscopy-based protein-miRNAs binding assay

5 µl of glutathione Sepharose 4B beads slurry (GE Healthcare) were added to a mixture of GST-fused bait proteins (GST-Cx43-NT, GST-Cx43-CT, GST-hnRNPA2B1 and/or GST-hnRNPQ, as indicated) and incubated for 1 h, at 4°C under agitation. In each experimental condition, the total amount of recombinant protein used was 20 µg (1:1:1 ratio, using GST in experimental conditions with only one bait protein). Beads were washed with 150 mM NaCl, 50 mM Tris at pH 7.4, after which they were resuspended in 6 µl of the same buffer. 10 µl of a 5 µM miRNAs prey solution (Cy3-miR-133b or

Cy3-miR-509-3p), was plated into the well of a 384-well glass-bottom microplate (Greiner Bio-One, Frickenhausen, Germany), after which 10% of the bait solution was added and allowed to equilibrate for 30 min. Specimens were imaged on a confocal microscope (Zeiss LSM 710, Carl Zeiss AG) with a Plan-Apochromat 20×/0.8 M27 objective (Carl Zeiss AG). As a measure of protein-miRNAs binding, total fluorescence/bead was quantified in maximal projection images (of acquired z-stacks), following background subtraction using ImageJ.

EV loading

5 μg of purified EV^{Cx43+} or EV^{Cx43-} were incubated with 10 μM SYTO® RNASelect™ green fluorescent stain (Thermo Fisher Scientific) for 20 min, at 37°C. Unincorporated dye was removed with Exosome Spin Columns (MW 3000; Thermo Fisher Scientific), according to manufacturer's instructions. Labeled EV were incubated with $HEK293^{Cx43+}$ for 30 min, at 37°C. Cells were fixed with 4% paraformaldehyde (PFA) and nuclei were stained with DAPI (4′,6-diamidino-2-phenylindole). Microscopy images were obtained using an Axio Observer.Z1 inverted microscope. Total fluorescence in EV-recipient cells was quantified using ImageJ, as a measure of EV-mediated transfer of fluorescent RNA.

Statistical analyses

Data represent are expressed as individual data points with mean ± SD. Independent variables were analyzed by Mann–Whitney test, whereas Kruskal–Wallis (Dunn's post hoc) was used for multiple comparisons. All analyses were performed with GraphPad Prism 6.01.

Data availability

This study includes no data deposited in external repositories. Data supporting the findings of this study are available from the authors upon reasonable request.

Expanded View for this article is available online.

Acknowledgements

Author contributions

Disclosure and competing interests statement

The authors declare that they have no conflict of interest.

References

Baer C, Lyle R, Burdet F, Gilfillan GD, De Palma M, Squadrito ML, Ibberson M, Maderna C (2014) Endogenous RNAs modulate microRNA sorting to exosomes and transfer to acceptor cells. *Cell Rep* 8: 1432–1446

Belter A, Gudanis D, Rolle K, Piwecka M, Gdaniec Z, Naskręt-Barciszewska MZ, Barciszewski J (2014) Mature miRNAs form secondary structure, which suggests their function beyond RISC. *PLoS One* 9: e113848

Cai X, Qu L, Yang J, Xu J, Sun L, Wei X, Qu X, Bai T, Guo Z, Zhu Y (2020) Exosome–transmitted microRNA-133b inhibited bladder cancer proliferation by upregulating dual-specificity protein phosphatase 1. *Cancer Med* 9: 6009

Catarino S, Ramalho JS, Marques C, Pereira P, Girão H (2011) Ubiquitin-mediated internalization of connexin43 is independent of the canonical endocytic tyrosine-sorting signal. *Biochem J* 437: 255–267

Fujita Y, Araya J, Ito S, Kobayashi K, Kosaka N, Yoshioka Y, Kadota T, Hara H, Kuwano K, Ochiya T (2015) Suppression of autophagy by extracellular vesicles promotes myofibroblast differentiation in COPD pathogenesis. *J Extracell Vesicles* 4: 28388

Fujiwara Y, Furuta A, Kikuchi H, Aizawa S, Hatanaka Y, Konya C, Uchida K, Yoshimura A, Tamai Y, Wada K *et al* (2013) Discovery of a novel type of autophagy targeting RNA. *Autophagy* 9: 403–409

Garcia-Martin R, Wang G, Brandão BB, Zanotto TM, Shah S, Kumar Patel S, Schilling B, Kahn CR (2022) MicroRNA sequence codes for small extracellular vesicle release and cellular retention. *Nature* 601: 446–451

Hellman LM, Fried MG (2007) Electrophoretic mobility shift assay (EMSA) for detecting protein-nucleic acid interactions. *Nat Protoc* 2: 1849–1861

Hobor F, Dallmann A, Ball NJ, Cicchini C, Battistelli C, Ogrodowicz RW, Christodoulou E, Martin SR, Castello A, Tripodi M *et al* (2018) A cryptic RNA-binding domain mediates Syncrip recognition and exosomal partitioning of miRNA targets. *Nat Commun* 9: 831

Koppers-Lalic D, Hackenberg M, Bijnsdorp I, van Eijndhoven M, Sadek P, Sie D, Zini N, Middeldorp J, Ylstra B, de Menezes R *et al* (2014) Nontemplated nucleotide additions distinguish the small RNA composition in cells from exosomes. *Cell Rep* 8: 1649–1658

Kozomara A, Griffiths-Jones S (2014) MiRBase: annotating high confidence microRNAs using deep sequencing data. *Nucleic Acids Res* 42: D68–D73

Kuleshov MV, Jones MR, Rouillard AD, Fernandez NF, Duan Q, Wang Z, Koplev S, Jenkins SL, Jagodnik KM, Lachmann A *et al* (2016) Enrichr: a comprehensive gene set enrichment analysis web server 2016 update. *Nucleic Acids Res* 44: W90–W97

Lee H, Li C, Zhang Y, Zhang D, Otterbein LE, Jin Y (2019) Caveolin-1 selectively regulates microRNA sorting into microvesicles after noxious stimuli. *J Exp Med* 216: 2202–2220

Leidal AM, Huang HH, Marsh T, Solvik T, Zhang D, Ye J, Kai F, Goldsmith J, Liu JY, Huang Y-H *et al* (2020) The LC3-conjugation machinery specifies the loading of RNA-binding proteins into extracellular vesicles. *Nat Cell Biol* 22: 187–199

Liao L, Chen Y, Zhou J, Ye J (2021) MicroRNA-133b inhibits nTumor Cell proliferation, migration and invasion by targeting SUMO1 in endometrial carcinoma. *Technol Cancer Res Treat* 20: 153303382110652

Martins-Marques T, Anjo SI, Pereira P, Manadas B, Girão H (2015a) Interacting network of the gap junction (GJ) protein Connexin43 (Cx43) is modulated by ischemia and reperfusion in the heart. *Mol Cell Proteomics* 14: 3040–3055

Martins-Marques T, Catarino S, Zuzarte M, Marques C, Matafome P, Pereira P, Girão H (2015b) Ischaemia-induced autophagy leads to degradation of gap junction protein connexin43 in cardiomyocytes. *Biochem J* 467: 231–245

Martins-Marques T, Catarino S, Gonçalves A, Miranda-Silva D, Gonçalves L, Antunes P, Coutinho G, Leite Moreira A, Falcão Pires I, Girão H (2020a) EHD1 modulates Cx43 Gap junction remodeling associated with cardiac diseases. *Circ Res* 126: E97–E113

Martins-Marques T, Pinho MJ, Zuzarte M, Oliveira C, Pereira P, Sluijter JPG, Gomes C, Girao H (2016) Presence of Cx43 in extracellular vesicles reduces the cardiotoxicity of the anti-tumour therapeutic approach with doxorubicin. *J Extracell Vesicles* 5: 32538

Martins-Marques T, Ribeiro-Rodrigues T, Batista-Almeida D, Aasen T, Kwak BR, Girao H (2019) Biological functions of Connexin43 beyond intercellular communication. *Trends Cell Biol* 29: 835–847

Martins-Marques T, Ribeiro-Rodrigues T, de Jager SC, Zuzarte M, Ferreira C, Cruz P, Reis L, Baptista R, Gonçalves L, Sluijter JPG *et al* (2020b) Myocardial infarction affects Cx43 content of extracellular vesicles secreted by cardiomyocytes. *Life Sci Alliance* 3: e202000821

McKenzie AJ, Hoshino D, Hong NH, Cha DJ, Franklin JL, Coffey RJ, Patton JG, Weaver AM (2016) KRAS-MEK signaling controls Ago2 sorting into exosomes. *Cell Rep* 15: 978–987

Mukherjee K, Ghoshal B, Ghosh S, Chakrabarty Y, Shwetha S, Das S, Bhattacharyya SN (2016) Reversible HuR-micro RNA binding controls extracellular export of miR-122 and augments stress response. *EMBO Rep* 17: 1184–1203

Perez-Hernandez D, Gutiérrez-Vázquez C, Jorge I, López-Martín S, Ursa A, Sánchez-Madrid F, Vázquez J, Yañez-Mó M (2013) The intracellular interactome of tetraspanin-enriched microdomains reveals their function as sorting machineries toward exosomes. *J Biol Chem* 288: 11649–11661

Popenda M, Szachniuk M, Blazewicz M, Wasik S, Burke EK, Blazewicz J, Adamiak RW (2010) RNA FRABASE 2.0: an advanced web-accessible database with the capacity to search the three-dimensional fragments within RNA structures. *BMC Bioinformatics* 11: 1–12

Popenda M, Szachniuk M, Antczak M, Purzycka KJ, Lukasiak P, Bartol N, Blazewicz J, Adamiak RW (2012) Automated 3D structure composition for large RNAs. *Nucleic Acids Res* 40: e112

Ribeiro-Rodrigues TM, Laundos TL, Pereira-Carvalho R, Batista-Almeida D, Pereira R, Coelho-Santos V, Silva AP, Fernandes R, Zuzarte M, Enguita FJ *et al* (2017a) Exosomes secreted by cardiomyocytes subjected to ischaemia promote cardiac angiogenesis. *Cardiovasc Res* 113: 1338–1350

Ribeiro-Rodrigues TM, Martins-Marques T, Morel S, Kwak BR, Girão H (2017b) Role of connexin 43 in different forms of intercellular communication—gap junctions, extracellular vesicles and tunnelling nanotubes. *J Cell Sci* 130: 3619–3630

Santangelo L, Giurato G, Cicchini C, Montaldo C, Mancone C, Tarallo R, Battistelli C, Alonzi T, Weisz A, Tripodi M (2016) The RNA-binding protein SYNCRIP is a component of the hepatocyte exosomal machinery controlling microRNA sorting. *Cell Rep* 17: 799–808

Sato K, Hamada M, Asai K, Mituyama T (2009) CentroidFold: a web server for RNA secondary structure prediction. *Nucleic Acids Res* 37: W277–W280

Shurtleff MJ, Temoche-Diaz MM, Karfilis KV, Ri S, Schekman R (2016) Y-box protein 1 is required to sort microRNAs into exosomes in cells and in a cell-free reaction. *Elife* 5: e19276

Soares AR, Martins-Marques T, Ribeiro-Rodrigues T, Ferreira JV, Catarino S, Pinho MJ, Zuzarte M, Isabel Anjo S, Manadas B, P.G. Sluijter J *et al* (2015) Gap junctional protein Cx43 is involved in the communication between extracellular vesicles and mammalian cells. *Sci Rep* 5: 13243

Sun Z, Ma Y, Chen F, Wang S, Chen B, Shi J (2018) miR-133b and miR-199b knockdown attenuate TGF-β1-induced epithelial to mesenchymal transition and renal fibrosis by targeting SIRT1 in diabetic nephropathy. *Eur J Pharmacol* 837: 96–104

Szklarczyk D, Gable AL, Lyon D, Junge A, Wyder S, Huerta-Cepas J, Simonovic M, Doncheva NT, Morris JH, Bork P *et al* (2019) STRING v11: protein-protein association networks with increased coverage, supporting functional discovery in genome-wide experimental datasets. *Nucleic Acids Res* 47: D607–D613

Temoche-Diaz MM, Shurtleff MJ, Nottingham RM, Yao J, Fadadu RP, Lambowitz AM, Schekman R (2019) Distinct mechanisms of microrna sorting into cancer cell-derived extracellular vesicle subtypes. *Elife* 8: e47544

Teng Y, Ren Y, Hu X, Mu J, Samykutty A, Zhuang X, Deng Z, Kumar A, Zhang L, Merchant ML *et al* (2017) MVP-mediated exosomal sorting of miR-193a promotes colon cancer progression. *Nat Commun* 8: 1–16

Théry C, Amigorena S, Raposo G, Clayton A (2006) Isolation and characterization of exosomes from cell culture supernatants and biological fluids. *Curr Protoc Cell Biol* 30: 1–3

Tishchenko A, Azorín DD, Vidal-Brime L, Muñoz MJ, Arenas PJ, Pearce C, Girao H, Cajal SRY, Aasen T (2020) Cx43 and associated cell signaling pathways regulate tunneling nanotubes in breast cancer cells. *Cancers* 12: 1–25

Tokar T, Pastrello C, Rossos AEM, Abovsky M, Hauschild AC, Tsay M, Lu R, Jurisica I (2018) MirDIP 4.1 - Integrative database of human microRNA target predictions. *Nucleic Acids Res* 46: D360–D370

Tomasello G, Armenia I, Molla G (2020) The protein imager: a full-featured online molecular viewer interface with server-side HQ-rendering capabilities. *Bioinformatics* 36: 2909–2911

van Balkom BWM, de Jong OG, Smits M, Brummelman J, den Ouden K, de Bree PM, van Eijndhoven MAJ, Pegtel DM, Stoorvogel W, Würdinger T *et al* (2013)

Endothelial cells require miR-214 to secrete exosomes that suppress senescence and induce angiogenesis in human and mouse endothelial cells. *Blood* 121: 3997–4006

Varela-Eirin M, Varela-Vazquez A, Rodríguez-Candela Mateos M, Vila-Sanjurjo A, Fonseca E, Mascareñas JL, Eugenio Vázquez M, Mayan MD (2017) Recruitment of RNA molecules by connexin RNA-binding motifs: implication in RNA and DNA transport through microvesicles and exosomes. *Biochim Biophys Acta Mol Cell Res* 1864: 728–736

Villarroya-Beltri C, Gutiérrez-Vázquez C, Sánchez-Cabo F, Pérez-Hernández D, Vázquez J, Martin-Cofreces N, Martinez-Herrera DJ, Pascual-Montano A, Mittelbrunn M, Sánchez-Madrid F (2013) Sumoylated hnRNPA2B1 controls the sorting of miRNAs into exosomes through binding to specific motifs. *Nat Commun* 4: 2980

Wang J, Rong Y, Ji C, Lv C, Jiang D, Ge X, Gong F, Tang P, Cai W, Liu W *et al* (2020) MicroRNA-421-3p-abundant small extracellular vesicles derived from M2 bone marrow-derived macrophages attenuate apoptosis and promote motor function recovery via inhibition of mTOR in spinal cord injury. *J Nanobiotechnol* 18: 1–17

Wolf P (1967) The nature and significance of platelet products in human plasma. *Br J Haematol* 13: 269–288

Yang D, Wan X, Dennis AT, Bektik E, Wang Z, Costa MGS, Fagnen C, Vénien-Bryan C, Xu X, Gratz DH *et al* (2021) MicroRNA biophysically modulates cardiac action potential by direct binding to ion channel. *Circulation* 143: 1597–1613

Zhou Y, Wang X, Song M, He Z, Cui G, Peng G, Dieterich C, Antebi A, Jing N, Shen Y (2019) A secreted microRNA disrupts autophagy in distinct tissues of *Caenorhabditis elegans* upon ageing. *Nat Commun* 10: 4827